Proceedings of the ASME 2010 3rd Joint US-European Fluids Engineering Summer Meeting and 8th International Conference on Nanochannels, Microchannels, and Minichannels
FEDSM-ICNMM2010
August 1-5, 2010, Montreal, Canada

FEDSM-ICNMM2010-30922

HEAT TRANSFER AND WAKE INTERACTION DYNAMICS FOR LOW MASS-DAMPING CYLINDER UNDERGOING FLOW-INDUCED VIBRATION AT HIGH REYNOLDS NUMBER

Amr Elbanhawy[1,2,*], **Ali Turan**[1]
[1]Energy and Multiphysics Group, School of Mechanical, Aerospace and Civil Engineering
University of Manchester, UK
PO Box 88, M60 1QD
[2]Energy Section, Dept. of Mechanical Engineering
Ain Shams University, Cairo, Egypt
Email: amr.elbanhawy@postgrad.manchester.ac.uk; ali.turan@manchester.ac.uk

ABSTRACT

The current open literature carries numerous publications about the dynamics of single structures freely oscillating in response to flow-induced forces of a cross-stream. Influence of controlled oscillations on heat transfer for relatively low Reynolds number cross-flow has been looked at previously, nonetheless, high Reynolds number measurements are difficult to obtain. Studies on the flow field in the vicinity of bodies with Flow-Induced Vibration (FIV) and its interaction with surface heat flux are what the current literature needs to enhance realization of such phenomenon and advance equipment design. The present study aims firstly at investigating the influence of cylinder's heat flux on (FIV) response and vice versa. Secondly, it explores the influence of high Reynolds number ($140,000$*) both on the cylinder's response and on heat transfer. An unsteady numerical framework is employed for the simulations, incorporating an Arbitrary Lagrangian Eulerian method for the associated grid deformation to simulate the coupled motion of the low mass-damping circular cylinder with a single degree of freedom in the initial regime. Attention is paid towards resolving the large scales of the fluid motion and the inherent coupling of the cylinder's motion towards the associated evolution of the time averaged flow field. The cylinder is assumed to have a constant heat flux while Large Eddy Simulation is used to solve for the turbulent flow field. Predictions show that significant changes occur to cylinder hydrodynamics and Reynolds stresses due to FIV. Wake mixing is enhanced and kinetic energy production field is qualitatively altered. Heat flux results in a noticeable increase in response amplitude for FIV cases while surface temperature and heat transfer coefficient undergo qualitative modifications in FIV scenario as opposed to a static cylinder. The variance of Nusselt number increases at parts of the cylinder's circumference due to FIV.*

NOMENCLATURE

f_n Cylinder natural frequency.
D Cylinder diameter.
$\bar{u},\bar{v};\bar{p}$ LES resolved "filtered" velocities and pressure respectively.
k_{sgs} Kinetic energy of Subgrid Scale "unresolved" structures.
μ Laminar kinematic viscosity.
$\overline{C_d}$ Cylinder time averaged drag coefficient.
St Cylinder Strouhal number.
θ_s^o Cylinder time averaged separation angle.
$\acute{C_l}$ Cylinder time averaged *total* lift fluctuation.
Pr_w Prandtl Number at cylinder surface.
$P_{(ke-p)}$ Kinetic energy production of resolved turbulent structures.

*Corresponding Author.

INTRODUCTION

It is widely recognized that Flow-induced Vibration (FIV) is a major concern in the design of modern mechanical equipment among which subsea risers and cross flow heat exchangers were given major attention. It is in fact no surprise to report that decades of recent research regarding the flow-structure interaction were essentially due to the significant damage caused by this very phenomenon. In particular with regards to cross-flow heat exchangers, the Electrical Energy Research Institute (EPRI) stresses that for large Heat Recovery Steam Generators (HRSGs), flow-induced vibration constitutes a major cause of equipment damage [1]. The current open literature carries numerous publications about the dynamics of single structures freely oscillating in response to flow-induced forces of a cross-stream. Nonetheless, studies on the flow field in the vicinity of such bodies are what the current literature needs to achieve an enhanced realization of such phenomenon and advance equipment design. This comes in special regard with high Reynolds number applications for which the interested community inquires about its influence on the single cylinder's response.

Studies for heat transfer around circular cylinders are extensively discussed in the literature [2]. It has been realized for decades that forced oscillations on a heated cylinder do enhance the heat flow from or to the cylinder surface; a phenomenon that relies on the fluid and temperature boundary layers around the cylinder. Pottebaum and Gharib [3] published a recent experimental study to further the investigations on the heat transfer from a single cylinder in cross flow from only transverse oscillations imposed on the cylinder. The enhancement in heat transfer was found to strongly depend on synchronization with harmonics of the natural shedding frequency, the cylinder wake mode and the cylinder's transverse oscillating velocity. This was accompanied by the fact that the eddy formation region was shortened; this is one of several factors affecting heat transfer as also highlighted in Zdravkovich [4] . Also, the effects of vorticity roll up and trajectories of shed vortices were found to affect heat transfer significantly in that such details explain how free-stream entrainment occurs. The velocity of the transverse oscillation was seen to affect greatly the heat transfer for it adds to the circulation and vorticity on the cylinder surface, and that does indeed enhance heat transfer.

In a complementary effort, Fu and Tong [5] numerically examined a similar case of a single heated cylinder with vertical oscillations in cross flow. The variations of the flow and thermal fields were classified into a class of moving boundary problems. An arbitrary Lagrangian - Eulerian kinematic description method was developed to describe the flow and thermal fields, whereas a finite element formulation was applied to solve the governing equations. The results showed that the interaction between the oscillating cylinder and vortex shedding dominates the state of the wake and that when the flow and thermal fields approach lock-in periodic regime, there was a remarkable enhancement in heat transfer. Park and Gharib [6] carried out another study for the effect of transverse oscillation on convective heat transfer for a single circular cylinder in cross flow. In their study, an experimental study was undertaken in water for a range of forced oscillation frequencies and at two amplitudes (0.1 and 0.2 of cylinder diameter). The Reynolds number was varied among 550, 1100 and 3500. A Digital Particle Image Velocimetry and Thermometry technique was used to gather data on flow field and heat transfer from the cylinder surface. It was found that besides the increase in heat transfer at the oscillation frequency corresponding to the Strouhal shedding frequency, there were other higher frequencies, namely super-harmonics, at which there was a large increase in the heat transfer. In particular, there was a large increase in heat transfer at approximately three times the unforced vortex shedding (Strouhal) frequency for amplitude ratio of 0.1. Also, there were large increases at approximately two and three times the frequency for an amplitude ratio of 0.2. Although the increase in heat transfer happened when the wake was in a state of synchronization with the oscillating frequency, the increase in heat transfer was essentially found to correlate inversely with the distance at which vortices roll up (eddy formation length). This matter is thought to be a necessary condition even if wake synchronization was achieved. As a result of the shortening of eddy formation region, the stagnant and low heat convecting fluid at the rear of the cylinder is refreshed. Finally, it was added that the large increases in heat transfer appeared to be the result of coherent motions of the wake, not turbulent or incoherent motions [6].

Pioneering work of Govardhan and Williamson [7] confirms that the maximum amplitude of a cylinder in transverse FIV increases as the Reynolds number increases. Following on this influence, a fluid-structure interaction scenario is investigated numerically herein for a turbulent flow past a circular cylinder at a very high subcritical Reynolds number. For validating an isothermal flow, two main experimental attempts by Cantwell and Coles [8] and Perrin et al. [9] were undertaken for a baseline Reynolds number of 140,000. This involves a stationary cylinder to study in detail the near wake mean flow and turbulence characteristics. These selected experiments conclusively show that the turbulent wake displays significant coherent structures of large eddies, possibly with stronger periodicity if the cylinder undergoes FIV as noted for a lower Reynolds number in Govardhan and Williamson's work [10]. Constant heat flux is then applied to the cylinder surface to investigate the subsequent effects on the vibration response and wake dynamics.

Large Eddy Simulation (LES) is employed with dynamic sub-grid scale modelling of Kim and Menon [11] for a two diameter span cylinder on static and freely rigid oscillating scenarios. With a single degree of freedom, the cylinder is modelled as a non-homogeneous mass-spring-damper system. The flow field and the cylinder are coupled in a fully explicit approach where a 4th order Runge-Kutta scheme is programmed to solve the cylinder system such that flow forces are fed to the cylinder lively through out the unsteady calculation. The simulation is undertaken by the commercial code Ansys-FLUENT where an Arbitrary Lagrangian Eulerian (ALE) deforming mesh technique is effectively incorporated to simulate a fluid-structure interaction problem. The cylinder response is compared against benchmark experiments of Brankovic and Bearman [12] for a single reduced velocity value of (2) in the initial regime. Structural properties are the same as that of Brankovic and Bearman [12]. In this work, the definition of reduced velocity as function of free stream velocity U_{in}, diameter D and natural frequency f_n follows as: $V_r = U_{in}D/f_n$. Details on the general dynamics of a freely oscillating single cylinder are discussed in Blevins [13].

MODELLING ASPECTS

A cell-centred finite volume method is used where gradients at cell centres are calculated via the Green-Gauss theorem as in Holmes and Connell [14]. Diffusive fluxes are discretized using a central differencing scheme. A bounded central differencing scheme is used to calculate the Navier-Stokes flow equations as applied by Leonard and Mokhtari [15]. First order backward-difference implicit time integration scheme is used with a non-dimensional time step of 0.0021 achieving a maximum value of one for Courant number. Discretized governing equations are solved using a point-implicit Gauss-Seidel relaxation, along with an algebraic multi-grid method as applied in Fluent code documentation [16]. A rectangular domain with 3.5 diameters upstream of the cylinder, 8.5 diameters downstream and 4.5 diameters on the top and bottom sides is utilised as in Fig. 1. The spanwise domain length is two diameters and the blockage ratio is 11.1%. The boundary layer zone of quadrilateral cells moves as a single entity with the cylinder when oscillating. It is designed to eliminate the need for turbulence wall functions and has a maximum circumferential wall non-dimensional distance Y^+ of one. This zone is followed by pyramidal elements for what is termed the dynamic mesh zone that is essential for the dynamic mesh motion incorporated herein. For the thermal boundary layer resolution, the definition of Nusselt number Nu at the cylinder surface entails that $\delta_T = D/Nu$, where δ_T is the thermal boundary layer thickness. For the current simulations, δ_T is represented with at least five grid points based on the maximum local Nu. Table 1 shows the grid resolution effects.

Filtered Navier-Stokes equations, continuity and energy transport equations are solved iteratively along with the equation for the Subgrid Scale stresses (SGS) [11]. For the incompressible flow assumed herein, the filtered Navier-Stokes equation is

$$\frac{\partial \overline{u_i}}{\partial t} + \frac{\partial \bar{u}_i \bar{u}_j}{\partial x_j} = -\frac{\partial}{\partial x_j}(\psi_{ij}) - \frac{\partial \overline{p}}{\partial x_i} - \frac{\partial \tau_{ij}}{\partial x_j} \tag{1}$$

where ψ_{ij} is the stress tensor due to molecular viscosity and τ_{ij} is the SGS stress defined by

$$\tau_{ij} \equiv \rho\overline{u_i u_j} - \rho\bar{u}_i\bar{u}_j. \tag{2}$$

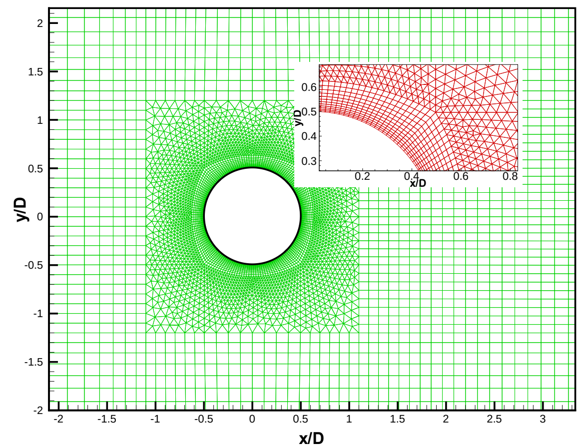

FIGURE 1: GRID TOPOLOGY FOR LES SIMULATIONS (2D SLICE).

The SGS stresses are modelled based on the Dynamic Kinetic Energy SGS Model devised by Kim and Menon [11] in which the turbulent viscosity μ_t is calculated from the SGS kinetic energy k_{sgs} as

$$\mu_t = C_k k_{sgs}^{0.5}\Delta_f, \tag{3}$$

and the SGS stresses are calculated from

$$\tau_{ij} - (2/3)k_{sgs}\delta_{ij} = -2C_k k_{sgs}^{0.5}\Delta_f\overline{S_{ij}}, \tag{4}$$

and k_{sgs} is found by solving its transport equation iteratively with the flow equations,

$$\frac{\partial \overline{k_{sgs}}}{\partial t} + \frac{\partial \bar{u}_j \overline{k_{sgs}}}{\partial x_j} = \frac{\partial}{\partial x_j}\left(\mu_t \frac{\partial k_{sgs}}{\partial x_j}\right) - C_\varepsilon \frac{k_{sgs}^{1.5}}{\Delta_f} - \tau_{ij}\frac{\partial \bar{u}_i}{\partial x_j}. \tag{5}$$

The rate-of-strain tensor $\overline{S_{ij}}$ is based on the resolved filtered velocity gradients. The filter size Δ_f is equivalent to cube root of cell volume. The C_k and C_ε are model constants determined dynamically [11]. As the boundary layer mesh is fine to resolve the laminar sublayer, the wall shear stress at the wall τ_w is simply determined as equal to $\mu\bar{u}/y_1$ where y_1 is the height of the first cell.

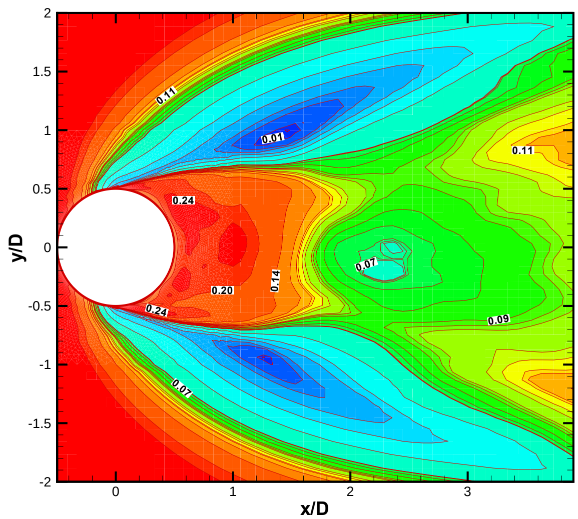

FIGURE 2: CONTOURS OF $K.E_{SGS}/K.E_{LES}$ MADE FOR THE 1^{st}*grid*.

Furthermore, the internal energy I equation with a turbulent Prandtl number Pr_t (here defined equal to 0.85), thermal conductivity k and specific heat C_p is represented as

$$\frac{\partial}{\partial t}(\rho I)+\frac{\partial}{\partial x_i}(\bar{u_i}\rho I)=\frac{\partial}{\partial x_j}\left((k+\frac{C_p\mu_t}{Pr_t})\frac{\partial T}{\partial x_j}\right). \quad (6)$$

The fluid used in the simulation is water with a reference temperature of 300 K; the Prandtl number Pr is about 6 while Richardson number Ri approaches $7.7e^{-07}$. The specific heat, thermal conductivity and viscosity are all temperature dependent as follows:

$$C_p = 4953.5-5.04T+0.0082T^2, \quad (7)$$

$$k = -0.484+0.00585T-7.34e^{-06}T^2, \quad (8)$$

$$\mu = 0.01278-6.5e^{-05}T+8.45e^{-08}T^2. \quad (9)$$

The inlet section has a constant velocity applied uniformly without any turbulent disturbances. A no-slip adiabatic condition is specified for the cylinder surface that is assumed to be perfectly smooth. At the outlet boundary, a fixed pressure value is maintained while all other flow variables are extrapolated from the interior. Symmetry condition is applied at the top, bottom and side boundaries such that gradients normal to their planes are set to zero. To study heat transfer effects on the wake and on the vibration response of the cylinder, a study heat flux of $1.85MW/m^2$ is applied to the cylinder surface.

TABLE 1: LES GRID STRUCTURE FOR SENSITIVITY ANALYSIS

Grid	Grid Points	Cylinder's 1^{st} cell $x/D, y/D, z/D$	Radial cell size increase ratio
1^{st}	1013868	1.3%, 0.016%, 5.5%	1.1
2^{nd}	2161391	0.96%, 0.016%, 4%	1.07

TABLE 2: PARAMETRIC COMPARISON OF GRID SENSITIVITY. EXPERIMENTS A AND B REFER TO REFERENCES [8] AND [9] RESPECTIVELY. THE EXPERIMENTAL RANGE IS TAKEN FROM REFERENCE [4] EXCEPT FOR $\overline{C_d}$ THAT IS FROM [8]. VALUES ARE NOT CORRECTED FOR EXPERIMENTAL SETUP

Grid	$\overline{C_d}$	θ_s^o	L_{rec}/D	$\acute{C_l}$	St
1^{st}	0.9	87.7	1.57	0.35	0.239
2^{nd}	1.12	83.8	1.43	0.37	0.216
1^{st}Heat Flux	0.83	88.7	1.64	0.235	0.25
Exp. A	1.237	–	1.1	–	0.179
Exp. B	1.44	–	1.23	–	0.21
Range (Exp)	0.85∼1.45	∼80	–	0.3∼0.6	0.18∼0.2

CYLINDER AND MESH MOVEMENT

An Euler integration is used to update the location of the cylinder as in the following equation: $X_{c.g}^{m+1} = X_{c.g}^{m}+v_{c.g}\delta t$. The vector $X_{c.g}$ indicates the position of the cylinder centre of gravity while $v_{c.g}$ indicates its velocity. With a single degree-of-freedom, the cylinder position is solved for the transverse direction. A fourth order Runge-Kutta integration scheme is used to solve the cylinder equation of motion with constant coefficients. The $m_{cyl.}$, c and k_s are the cylinder mass, damping and stiffness coefficients respectively as used in the equation of motion

$$m_{cyl.}\ddot{y}+c\dot{y}+k_s y = F_{fluid-y-direction}. \quad (10)$$

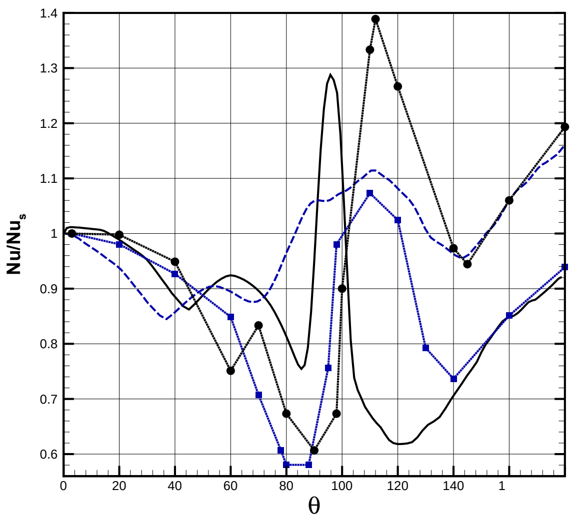

FIGURE 3: TIME AVERAGED LOCAL NORMALIZED Nu AGAINST DATA FROM [20]. SOLID LINE (LES-STATIC); DASHED LINE (LES-FIV); • $Re = 170000$ [20]; ▪ $Re = 140000$ [20].

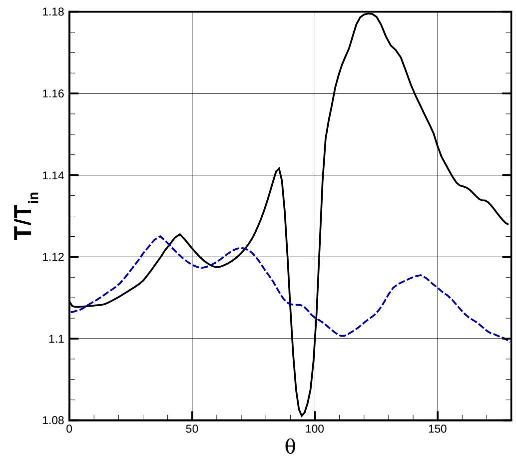

FIGURE 4: TIME AVERAGED NORMALIZED WALL TEMPERATURE. SOLID LINE (LES-STATIC); DASHED LINE (LES-FIV).

The cylinder location is determined after fully solving for the flow field at every time step. The cylinder acquires its motion from integrated pressure and shear stresses of the fluid domain as seen on the right hand side of the equation above. Parameters for identifying the structural properties and their relations are as follows:

- Specific mass:$m^* = 4m_{cyl.}/(\pi D^2 \rho_{fluid} l)$, where l is the cylinder's length.
- Mass damping:$m^*\zeta$, ζ is the damping ratio that is related to the cylinder's damping coefficient by the expression: $c = 2\zeta\sqrt{k_s m_{cyl}}$.

The Arbitrary Lagrangian-Eulerian (ALE) technique handles the mesh motion where grid points are realized as springs with fictitious stiffness and updated at every time step. If the updated cell size or skewness is less or greater than the set limits, the cell is agglomerated or split "re-meshed" respectively. A limit is set that adopts 50% allowable deviation for the cell shape from an equilateral triangle. The minimum and maximum cell sizes are 1.2% and 4.5% of the cylinder diameter respectively. Mesh deformation is not allowed in the boundary layer zone surrounding the cylinder in order to avoid possible interpolation errors around the area where delicate separation occurs. The Space Conservation Law (SCL) is applied as demonstrated by Farhat et al. [17]. When cell deformation occurs, field values are derived by spatial interpolation; this would provide the initial values before iteration takes place at every time step.

RESULTS AND ANALYSIS

Numerical predictions for a freely oscillating cylinder are compared against lab-based measurements of Brankovic and Bearman [12] with and without the cylinder's surface heat flux. The specific mass for the experiment of Brankovic and Bearman is 0.82 while the damping ratio is $1.5e^{-4}$. Beforehand, however, a study for a stationary cylinder is presented also with isothermal and heat transfer scenarios. This is to establish credible grid sensitivity while isolating the influence of dynamic meshing. Grid sensitivity studies are shown in Table 2. The drag coefficient is better predicted by the fine grid and this is more likely due to the finer spanwise resolution as also noted by Breuer [18] in a similar LES study. For the two LES grids tested, there is a general tendency to over-predict the time averaged separation angle at the middle section of the cylinder span. Such overprediction has also been reported for an LES study [18] although it was stressed that a significant scatter exists with a nonlinear relationship between Re and θ_s^o at high precritical Reynolds number. The overprediction of the recirculation length L_{rec} is a result of the delayed separation and the consequent higher base pressure. The coexistence of high St, low mean drag and longer L_{rec} has also been reported by Travin et al. [19] in their coarse DES studies on the same Re number. There is a reasonable prediction of the fluctuating lift $\acute{C}_l$; it is important to note here that the values of fluctuating lift here are *total* and based on the entire span of the cylinder model. The Strouhal number St is better predicted by the finer grid; its overprediction by the coarse grid agrees with the findings of Breuer [18]. The authors suppose that the difference in St prediction is mainly due to the better spanwise resolution offered by the fine grid.

Heat flux scenario is only applied on the coarse grid showing significant differences from its isothermal counterpart. Mean

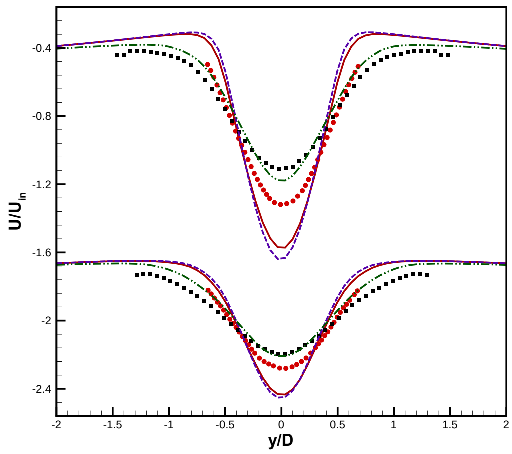

(a)

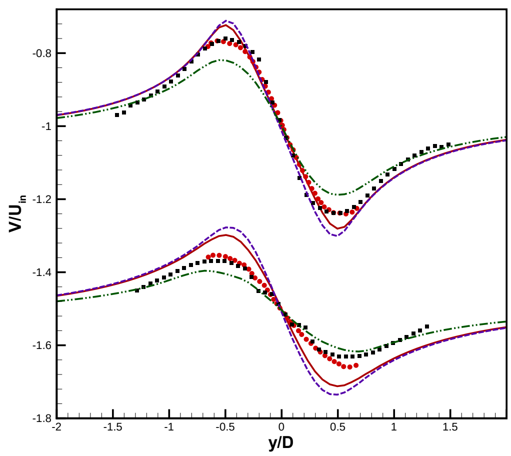

(b)

FIGURE 5: NORMALIZED TIME-AVERAGED VELOCITIES AT $x/D =$ 1.5 AND 2.0 (FROM TOP TO BOTTOM RESPECTIVELY) COMPARED AGAINST EXPERIMENTAL DATA. SOLID LINE (LES-STATIC); DASHED LINE (LES-STATIC-HEATED); DASH-DOT LINE (LES-FIV-HEATED); ▪ CANTWELL AND COLES [8]; • PERRIN ET AL. [9]

drag and fluctuating lift have decreased while there is an increase in St accompanied by longer L_{rec} that is also caused by the SGS viscosity generated in the immediate wake. For the coarse grid, Fig. 2 shows the percentage of SGS kinetic energy to the resolved (filtered) kinetic energy in order to indicate regions of high SGS viscosity generation. Meanwhile, for better computational efficiency out of the tested grids, the following discussion exclusively concentrates on the first grid (i.e., coarse grid) for studying the effects of heat transfer and FIV response. The Nusselt number in the front stagnation point is equal to 911.5 if calculated for the static cylinder from the empirical relation [2]: $Nu_{fs} = 1.11Re^{0.5}Pr^{0.35}(Pr/Pr_w)^{0.25}$. The current simulation gives 870.

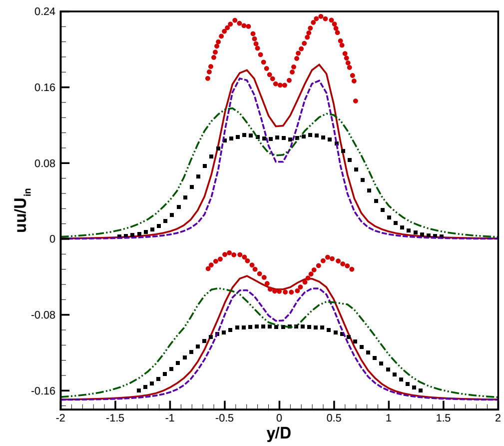

(a)

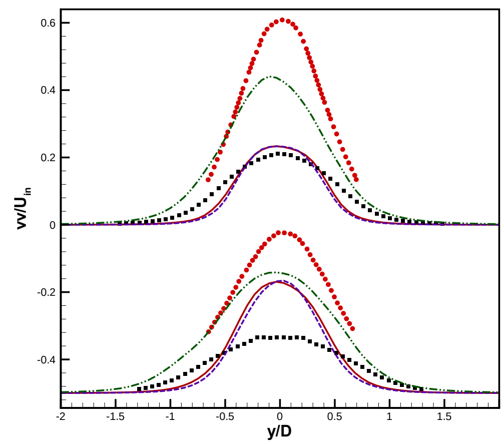

(b)

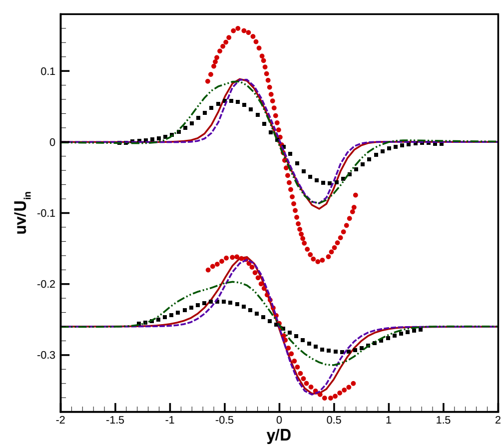

(c)

FIGURE 6: NORMALIZED TIME-AVERAGED REYNOLDS STRESSES AT $x/D = 1.5$ AND 2.0 (FROM TOP TO BOTTOM RESPECTIVELY) COMPARED TO EXPERIMENTAL DATA. SOLID LINE (LES-STATIC); DASHED LINE (LES-STATIC-HEATED); DASH-DOT LINE (LES-FIV-HEATED); ▪ CANTWELL AND COLES [8] (*global*); • PERRIN ET AL. [9] (*global*)

The average Nusselt number equals 723.38 if calculated -also for the static cylinder- empirically [2]: $\overline{Nu} = 0.26Re^{0.6}Pr^{0.37}(Pr/Pr_w)^{0.25}$. The current simulation shows a value of 748.12. Figure 3 shows the local distribution of time averaged Nu around the upper surface of the cylinder compared to two other experiments made with air, $Pr = 0.7$, by Giedt [20]. It is shown that the LES results for a static cylinder capture the overall trends showing maximum heat transfer following separation in the high precritical Re range. Furthermore, $\overline{Nu}$ of the freely oscillating cylinder shows a value of 880.2 exceeding that of the static cylinder. It is also evident how transverse oscillation alters local Nu distribution both quantitatively and qualitatively showing a predominant increase post separation. Subsequently, Fig. 4 shows temperature distribution around the circumference of the cylinder showing a decreased surface temperature at the rear end of the cylinder when it undergoes flow induced vibration.

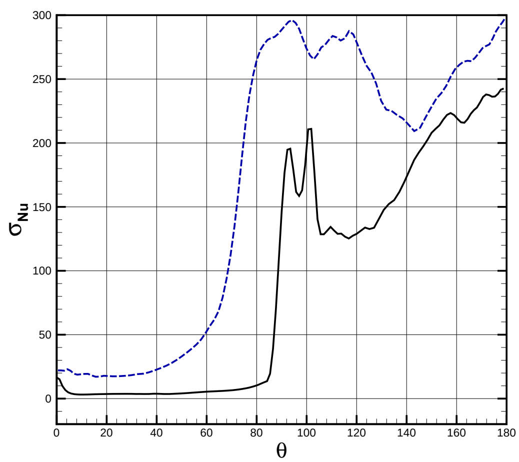

FIGURE 7: STANDARD DEVIATION OF LOCAL Nu. SOLID LINE (LES-STATIC-HEATED); DASHED LINE (LES-FIV-HEATED).

Average streamwise and transverse velocity profiles at near wake cross-sections are shown on Fig. 5. Overprediction of the recirculation bubble results in LES values showing deviation from both experimental attempts. However, agreements tends to be closer on the $2D$ cross-section. Here the effect of heat flux shows greater velocity deficit that coincides with the longer recirculation bubble predicted (Table 2). LES predictions for transverse velocity show better agreement on the $1.5D$ channel, yet, a sustained overprediction at $2.0D$ due to the longer recirculation bubble. For the heat flux scenario, transverse flow-Induced Vibration (FIV) has caused a significantly shorter recirculation bubble with more free-stream entrainment as inferred

TABLE 3: CHARACTERISTICS OF FLOW-INDUCED VIBRATION RESPONSE

Case	y_{cyl}/D	$\Delta\Phi°$	f_{osc}/f_n
Brankovic and Bearman [12]	0.13	0°	0.47
Heated Oscil. Cyl.(CFD)	0.12	0°	0.414
Oscil. Cyl.(CFD)	0.12	0°	0.41

from the lower mean velocity deficit (peak variation along the cross-section). The shorter L_{rec} agrees with what Govardhan and Williamson [10] found for a FIV cylinder in the initial regime.

The turbulent flow around the cylinder is decomposed, as an arbitrary instantaneous quantity s, into a global average, a phase average and an instantaneous or random component as

$$s(x,y,t) = \bar{s} + \tilde{s} + \acute{s}. \qquad (11)$$

For the LES results herein, resolved stresses or velocity fluctuations combine both the phase average and the instantaneous for what is termed *global*. LES computations do not capture the whole spectrum of energy for the fluctuating velocities, however, Fig. 2 shows that *SGS* component is vanishing downstream the near wake. Comparisons are hence made also at wake cross-sections $1.5D$ and $2D$ shown on Fig. 6. For the streamwise stresses, LES static predictions generally follow the trend in Perrin et al. [9] due to the high blockage ratio and subsequent longer L_{rec} shown in [9]. Accord is enhanced at $2.0D$, perhaps due to the higher effect of *SGS* viscosity at $1.5D$ that may have directly decreased the width of spreading of $\overline{uu}$ across the wake. At $1.5D$ the transverse stresses approach the values in [8] while they are underpredicted with respect to Perrin et al. [9] data. Better agreement, however, is shown at $2.0D$ channel. Taking into account the longer recirculation bubble, it is noteworthy to indicate that such wake spatial difference would certainly affect the results. It may be expected to see the $\overline{vv}$ stress closer to Perrin et al. [9] due to that the current computational domain does not offer the same span and blockage as in [8]. With this rationale, $\overline{vv}$ is likely underpredicted by SGS viscosity produced near the base of the cylinder. At $2.0D$, LES static results fall closer to Perrin et al. [9] but is higher than that in [8]. This overprediction in $\overline{vv}$ compared to [8] has also been reported by Breuer [18]. The LES static results for shear stress $\overline{uv}$ is generally higher than that reported in [8]. The overprediction of shear stress in $2.0D$ is due to that this distance falls at the end of the recirculation bubble.

For the static cylinder, heat flux reduces the peaks of $\overline{uu}$

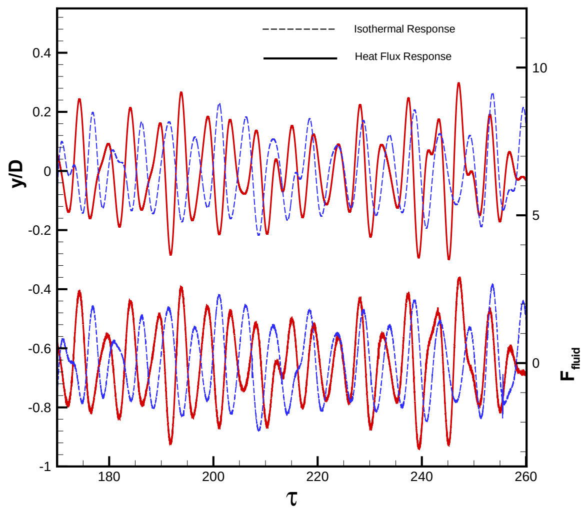

FIGURE 8: TIME SERIES OF NORMALIZED FIV DISPLACEMENT AND LIFT FORCE PREDICTED BY LES. SOLID LINE (LES-FIV-HEATED); DASHED LINE (LES-FIV).

without other marked influences on $\overline{vv}$ or $\overline{uv}$. For FIV scenario with heat flux, there seems marked *peaks* decrease of $\overline{uu}$, increase of $\overline{vv}$ -as expected from the transverse motion- and a limited decrease in $\overline{uv}$ for $2.0D$. It is evident here how the spreading of all fluctuations is enhanced along the cross-section; this indicates better mixing and entrainment. Unsteady heat transfer is very important for the determination of effectiveness and structural integrity for heat transfer equipment. In Fig. 7, the standard deviation of Nu is plotted for both the static and FIV scenarios. Most of the fluctuations in Nu occur in the rear part of the cylinder. It is interesting to see the onset of sharp increase in fluctuations at boundary layer separation with even a maximum at the rear stagnation point. Such behaviour does not qualitatively differ for the oscillating cylinder in the initial regime with $2S$ shedding pattern. Quantitatively, oscillations greatly improve heat transfer around the entire surface. Interestingly, the sudden increase of σ_{Nu} for the FIV cylinder does not match with the averaged separation angle listed in Table 2. In fact, this occurs in more than 10° earlier than mean separation. Although it remains higher than its static counterpart, σ_{Nu} profile shows a downward slope at 120° until it rises again at 142°. The LES results of the cylinder's response to FIV are shown in terms of normalized transverse displacement and lift force on Fig. 8. It is peculiar to see that despite the lower fluctuations in lift force exhibited by a static heated cylinder, heat flux increases fluctuations in lift force in FIV situation. Consequently, this results in higher peaks of transverse displacement time series for what is termed the heat flux response. Figure 9 shows the Fourier Fast Transform (FFT) spectral analysis of the displacement signal with and without heat flux. While both cases exhibit almost the same dominant frequency, heat flux causes the response to exhibit secondary -although minor- responses at different frequencies.

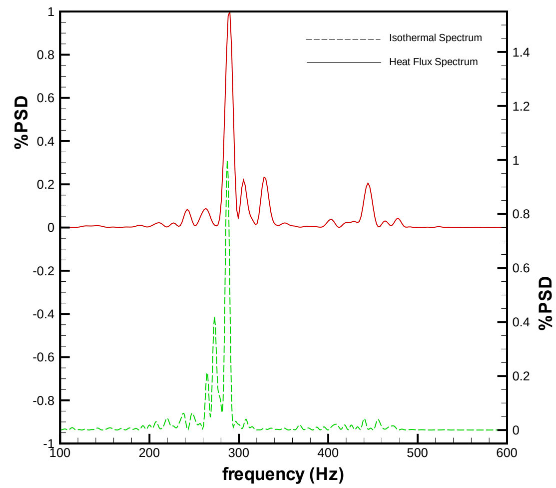

FIGURE 9: FFT ANALYSIS OF DISPLACEMENT AND FORCE SPECTRA PREDICTED BY LES. SOLID LINE (LES-FIV-HEATED); DASHED LINE (LES-FIV).

Table 3 shows the response characteristics compared between current LES predictions and results from Brankovic and Bearman [12]. It is essential to note here that Brankovic and Bearman [12] made their test at $Re \approx 4000$ for the reduced velocity of concern herein (i.e., 2). Favourably, the predicted phase angle $\Delta\Phi°$ in between the fluid force and the cylinder vertical response is zero. Also, the amplitude at the dominant harmonic is in close accord with its experimental counterpart, however, the time series show instantaneous amplitudes as high as $0.27D$ and $0.3D$ with and without heat flux respectively. Frequency ratio is underpredicted by around 13% compared to the value experimentally obtained; it is either a Re effect or modelling error that needs to be investigated further.

Turbulence production $P_{(ke-p)}$ is evaluated from the main stream to the resolved eddy motion, with $\partial\overline{u}/\partial x$ being flow gradients and $\overline{u_i u_j}$ being the time averaged resolved Reynolds stresses, as follows:

$$P_{(ke-p)} = -\overline{u_i u_j}\frac{\partial\overline{u}_i}{\partial x_j}. \quad (12)$$

Figure 10 shows the contours of LES resolved turbulent energy production for the static and oscillating heated cases respectively. The qualitative and quantitative distribution of turbulent

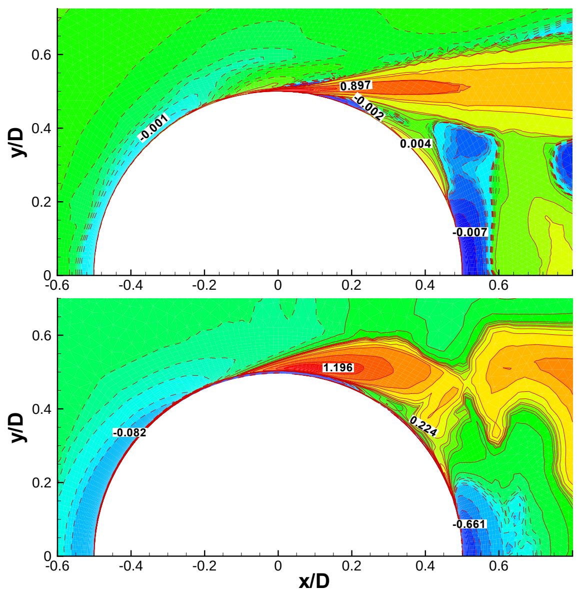

FIGURE 10: CONTOURS OF TIME AVERAGED NORMALIZED KINETIC ENERGY PRODUCTION $P_{(ke-p)}$ BY LES. TOP: STATIC CYLINDER; BOTTOM: FIV-CYLINDER

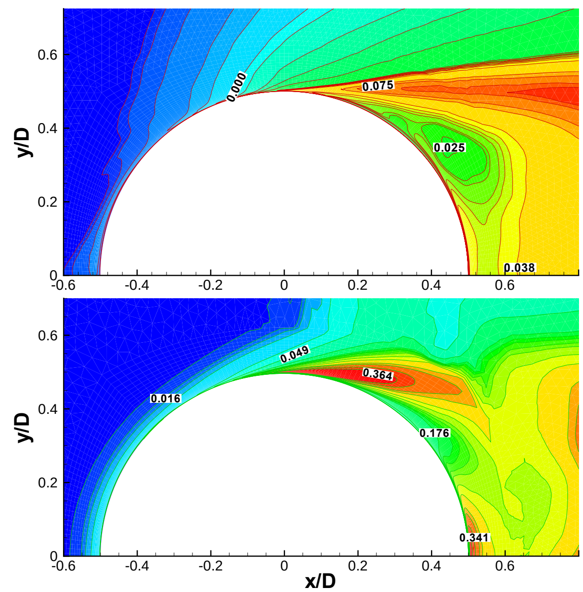

FIGURE 11: CONTOURS OF TIME AVERAGED NORMALIZED KINETIC ENERGY OF FLOW PREDICTED BY LES. TOP: STATIC CYLINDER; BOTTOM: FIV-CYLINDER.

energy production differs significantly nearer the cylinder boundary layer than is the case further downstream. For the static case, the thin boundary layer before separation -perhaps not quite clear here- has positive energy production, the maximum of which lies in the separated shear layer, augmenting the eddy structures. The base of the cylinder has a region of negative production zone that serves as a sink for the energy of the resolved eddy structures. Contrary to such, for the oscillating case, the thin boundary layer area is almost dominated by negative production (destruction of energy of eddy structures). However, away from the thin boundary layer area, there is a region of strong energy production as part of the separated shear layer. The time averaged kinetic energy of the resolved structures is plotted on Fig. 11. Similar to $P_{(ke-p)}$, the cylinder oscillations have caused a significant increase -by not less than an order of magnitude- in the kinetic energy. This increase is more pronounced in the separated shear layers and in the cylinder's base. This coincides with the enhanced base heat transfer earlier discussed.

CONCLUSIONS

The cylinder's wake for the studied Reynolds number (140000) exhibits distinct vortical structures that are amenable to resolution by means of Large Eddy Simulation. The cylinder free oscillation enhances free stream entrainment into the wake and results in changes to the *global* Reynolds stresses. When applied to the cylinder surface, heat flux induces some changes to the vibration response of the cylinder. In the studied "initial regime", flow-induced vibration enhances heat transfer significantly and especially in the rear half of the cylinder. Furthermore, significant changes in kinetic energy and its production occur around the cylinder boundary especially in the separated shear layer and at the cylinder base.

ACKNOWLEDGMENT

The authors would like to acknowledge the research fund by a scholarship from University of Manchester. Gratitude is due to the courtesy and assistance from Dr. A. Revell and Prof. M. Braza for the access of experimental data used for validation.

REFERENCES

[1] EPRI Technical Report No. 1004240, 2003. Delivering high reliability heat recovery steam generators. URL `http://my.epri.com/portal`.

[2] Zukauskas, A., and Ziugzda, J., 1986. *Heat transfer of a cylinder in cross flow*. Hemisphere.

[3] Pottebaum, T. S., and Gharib, M., 2006. "Using oscillations to enhance heat transfer for a circular cylinder". *Intl. Journal of Heat and Mass Tansfer,* ***49***, pp. 3190–3210.

[4] Zdravkovich, M. M., 1997. *Flow around circular cylinders: a comprehensive guide through flow phenomena. Vol.1: Fundamentals*. Oxford University Press, Oxford.

[5] Fu, W. S., and Tong, B. H., 2002. "Numerical investigation of heat transfer from a heated oscillating cylinder in a cross flow". *Intl. Journal of Heat and Mass Tansfer*, ***45***, pp. 3033–3043.
[6] Park, H. G., and Gharib, M., 2001. "Experimental study of heat convection from stationary and oscillating circular cylinder in cross flow". *ASME Journal of Heat Tansfer*, ***123***, pp. 51–62.
[7] Govardhan, R., and Williamson, C. H. K., 2006. "Defining the 'modified griffin plot' in vortex-induced vibration: revealing the effect of reynolds number using controlled damping". *Journal of Fluid Mechanics*, ***561***, pp. 147–180.
[8] Cantwell, B., and Coles, D., 1983. "An experimental study of entrainment and transport in the turbulent near wake of a circular cylinder". *Journal of Fluid Mechanics*, ***136***, pp. 321–374.
[9] R. Perrin and M. Braza and E. Cid and S. Cazin and F. Moradei and A. Barthet and A. Sevrain and Y. Hoarau", title = "Near-wake turbulence properties in the high Reynolds number incompressible flow around a circular cylinder measured by two-and three-component PIV", 2006.". *Journal of Flow, Turbulence and Combustion*, ***77***, pp. 185–204.
[10] Govardhan, R., and Williamson, C. H. K., 2001. "Mean and fluctuating velocity fields in the wake of a freely-vibrating cylinder". *Journal of Fluids and Structures*, ***15***, pp. 489–501.
[11] Kim, W. W., and Menon, S., 1997. "Application of the localized dynamic subgrid-scale model to turbulent wall-bounded flows". In Technical Report AIAA-97-0210, 35th Aerospace Sciences Meeting, American Institute of Aeronautics and Astronautics.
[12] Brankovic, M., and Bearman, P. W., 2006. "Measurements of transverse forces on circular cylinders undergoing vortex-induced vibration". *Journal of Fluids and Structures*, ***22***, pp. 829–836.
[13] Blevins, R. D., 1994. *Flow-Induced Vibration. 2nd Edition*. Krieger Publishing Company, Florida.
[14] Holmes, D. G., and Connell, S. D., 1989. "Solution of the 2d navier-stokes equations on unstructured adaptive grids". AIAA 9th CFD Conference, American Institute of Aeronautics and Astronautics.
[15] Leonard, B. P., and Mokhtari, S., 1990. ULTRA-SHARP Nonoscillatory Convection Schemes for High-Speed Steady Multidimensional Flow. Tm 1-2568 (icomp-90-12), NASA, NASA Lewis Research Center.
[16] Fluent, 2010. *Theory Guide*, latest ed. ANSYS Inc., Canonsburg, PA,USA.
[17] Farhat, C., Geuzaine, P., and Grandmont, C., 2001. "The discrete geometric conservation law and the nonlinear stability of ALE schemes for the solution of flow problems on moving grids". *Journal of Computational Physics*, ***174***, pp. 669–694.
[18] Breuer, M., 2000. "A challenging test case for large eddy simulation: high Reynolds number circular cylinder flow". *Intl. Journal of Heat and Fluid Flow*, ***21***, pp. 648–654.
[19] Travin, A., Shur, M., Strelets, M., and Spalart, P., 1999. "Detached-eddy simulations past a circular cylinder". *Journal of Flow, Turbulence and Combustion*, ***63***, pp. 293–313.
[20] Giedt, W. H., 1949. "Investigation of variation of point unit-heat transfer coefficient around a cylinder normal to an air stream". *Transactions of ASME*, ***71***, pp. 375–381.